Chemical Imaging by Dissolution Analysis (CIDA): Localized Kinetics of Dissolution Behavior to Provide 2D Chemical Mapping and Tomographic Imaging on a Nanoscale

Michael Reading [1*], Muhammad U. Ghori [2], D. Robert Brown[1], Leigh T. Fleming [3], Milan D. Antonijevic [4], David B. Grandy [5], Douglas J. Hourston [5], Mo Song [5], Barbara R. Conway [2]

[1]Department of Chemical Sciences, School of Applied Sciences, University of Huddersfield, Queensgate, Huddersfield, HD1 3DH, UK.

[2]Department of Pharmacy, School of Applied Sciences, University of Huddersfield, Queensgate, Huddersfield, HD1 3DH. UK

[3]Mechanical and Automotive Engineering, School of Computing and Engineering, University of Huddersfield, Queensgate, Huddersfield, HD1 3DH, UK[4]

[4]Faculty of Engineering and Science, University of Greenwich, Central Avenue, Chatham Maritime, ME4 4TB, UK

[5]Loughborough University, Epinal way, Loughborough LE11 3TU, UK

*M.Reading@hudd.ac.uk

ABSTRACT: A new approach to achieving chemical mapping on a nanoscale is described that can provide 2D and tomographic images of surface and near-surface structure. The method comprises dissolving material from the surface of the sample by applying a series of aliquots of solvent then analyzing their contents after removing them, in between exposures the surface is imaged with atomic force microscopy. This technique relies on being able to compensate for any drift between images by use of software. It was applied to a blend of two polymers, PMMA and PS. The analytical data identified the material that was dissolved and the topography images enabled the location of the various materials to be determined by analyzing local dissolution kinetics. The prospects for generalizing the approach are discussed.

INTRODUCTION

Chemical mapping is routinely used to study the structure and functionality of a wide range of materials[1,2,3]. In very general terms, the desirable capabilities for a chemical imaging method include:-

I. The ability to achieve high spatial resolution (preferably down to nanometres)
II. The ability to contend with thick samples and samples with rough surfaces with minimal sample preparation
III. The ability to use more than one analytical technique to probe the composition of a selected region of the sample. In particular, it is useful to determine whether it contains a mixture of compounds or only one type of molecule.
IV. The ability to provide detailed chemical information as a function of depth (preferably tomography)

This is not an exhaustive list as there can be other considerations; however, these are the principal capabilities most analytical scientists find useful for addressing a wide variety of samples. There is a range of established conventional techniques that can be used for chemical mapping[1,2,3], however, here we will confine the scope of our discussion to the more recent SPM-based techniques[4]. There is a growing number of these, some of which are commercially available. They fall into two categories: thermomechanical photothermal Nano-IR techniques and tip-enhanced scattering techniques[4]; both of these are non-destructive, an advantage in some cases, but there are fundamental obstacles to either enabling tomography. The former, when used with top-down illumination[5,6,7], shows promise (illuminating the sample from below precludes the possibility of looking at thick samples and obtaining depth information). However, current implementations still require that samples are thin and interpreting depth information is not yet possible (we return to this point in the discussion section when considering tomographic imaging). Tip-enhanced scattering techniques[4,8] can achieve the highest lateral spatial resolution, circa 20 nm, because the measured signal is dominated by the enhanced field around the tip. By the same token, they probe only the top 20 nm of the sample and cannot, therefore, provide depth information.

There is a versatile family of techniques pioneered by Reading, Price, Hammiche, Pollock and their co-workers.[9-12] that use thermal probes. The techniques include local volatilization/pyrolysis using a heated tip with subsequent analysis of the evolved gases by MS or GPC-MS[9,12], both depth profiling[12] and imaging[13,14,15] have been demonstrated. Spatial resolution is currently limited to micrometers[15]; this limit is, in part, imposed by the sensitivity of the mass spectroscopy instruments used to date thus higher spatial resolution will probably be possible. Like CIDA (see below) these MS-based approaches are locally destructive; material is removed thereby allowing access to the material below for subsequent analysis[12]; in principle, this provides for tomography[12]. However, an obstacle arises because this newly exposed material might have been changed by its recent exposure to elevated temperatures, this could lead to intractable complications. For example, charring would represent a substantial chemical change and prevent further

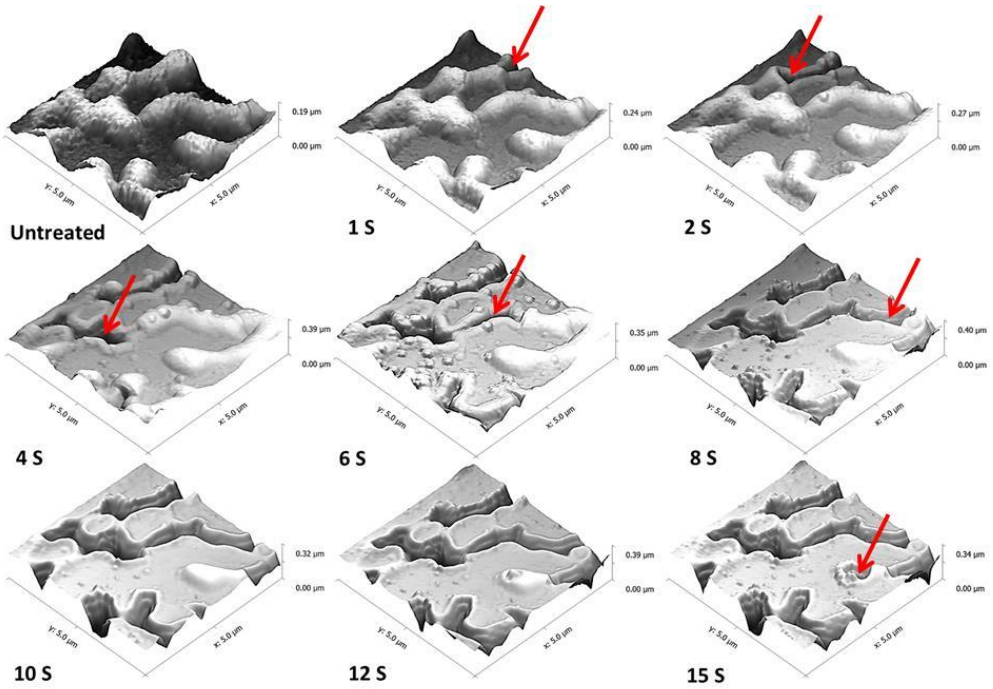

Figure 1. Images of a selected region showing how material is removed from the surface in a series of steps; the scale is 5µm x 5µm. The red arrows indicate an area where there is a sudden removal of material resulting in a pit or trough compared to the previous image.

pyrolysis. When using solvents to remove material, as is the case with CIDA, this complication is avoided. In addition to MS and GPC-MS, heated thermal tips can be used for local thermal analysis[12] (with the possibility of tomography[16]) and IR photothermal spectroscopy[11,12], (with the possibility of imaging[7] and depth profiling[7]). Although tomography has been achieved using local thermal analysis[16], this provides no chemical information except, perhaps, indirectly. Although imaging and depth profiling have been achieved using this type of thermal-tip-based photothermal spectroscopy, a fundamental problem is that true tomography would require the solution of the inverse problem. There are currently no indications progress is being made with this.

An extension of the thermal probe methods is thermally-assisted nanosampling[10,12,14,17]. It can enable femtogram quantities of material to be taken from a surface and analyzed by MS[14], IR[7,17] and even chromatographic techniques,[18] thus mixtures can be separated. This interesting combination of capabilities does offer the possibility of tomography, however, it has not yet entered the mainstream of analytical science and so will not be further considered here.

A consideration that is important in the context of this article is the ability to analyze real-world samples; this is one of the principal goals of our research. It is difficult to provide a rigorous definition of what a "real-world" sample is, but we can consider them to be those that are derived from materials that are present in our everyday environment, such as polymer composites, pharmaceutical dosage forms, packaging, coatings, etc. (excluding biological samples at this time). There is another important consideration when dealing with these samples; nanoscale scrutiny is usually only useful if the structure of the region that is imaged is representative of a much larger area, typically orders of magnitude larger. If it were the case that a surface comprised a vast array of chemically different nano-domains, it would take a prohibitively long time to characterize it with any of the SPM-based methods. In general, samples possibly have nanoscale structures, but these structures are almost always substantially the same over areas of square millimeters or even, in the case of coatings, square meters. We exploit this fact in our method.

In this article we present a new paradigm for surface characterisation and 3D-chemical mapping down to the nanoscale. It consists of exposing the surface of a sample to a succession of aliquots of a liquid so that materials are gradually removed from the surface. Using atomic force microscopy with suitable image processing software, changes in the topography of the surface are measured. A decrease in height is a measure of the loss of material from the surface to the liquid, this translates to a measure of the kinetics of the surface dissolution/erosion process, i.e. where we see rapid loss, there is a high rate of dissolution/reaction/erosion, gradual loss equates to slow kinetics (integrating decrease in height over selected areas gives a measure of volume loss). The species taken up by the solvent are analysed by any appropriate analytical method, from this we have a second measure of the kinetics of the dissolution/reaction/erosion process. The AFM data provide the location associated with kinetics, the analytical data provide chemical composition associated with kinetics. By correlating these two sets of data, i.e. rate of volume loss from the surface with quantity measured in each aliquot of the solvent, we can achieve a map of the location of the identified materials in 3D. We have demonstrated this method using a polymer blend comprising 30% w/w polystyrene (PS) and 70% poly (methylmethacrylate), (PMMA) with analytical information provided by FTIR.

.

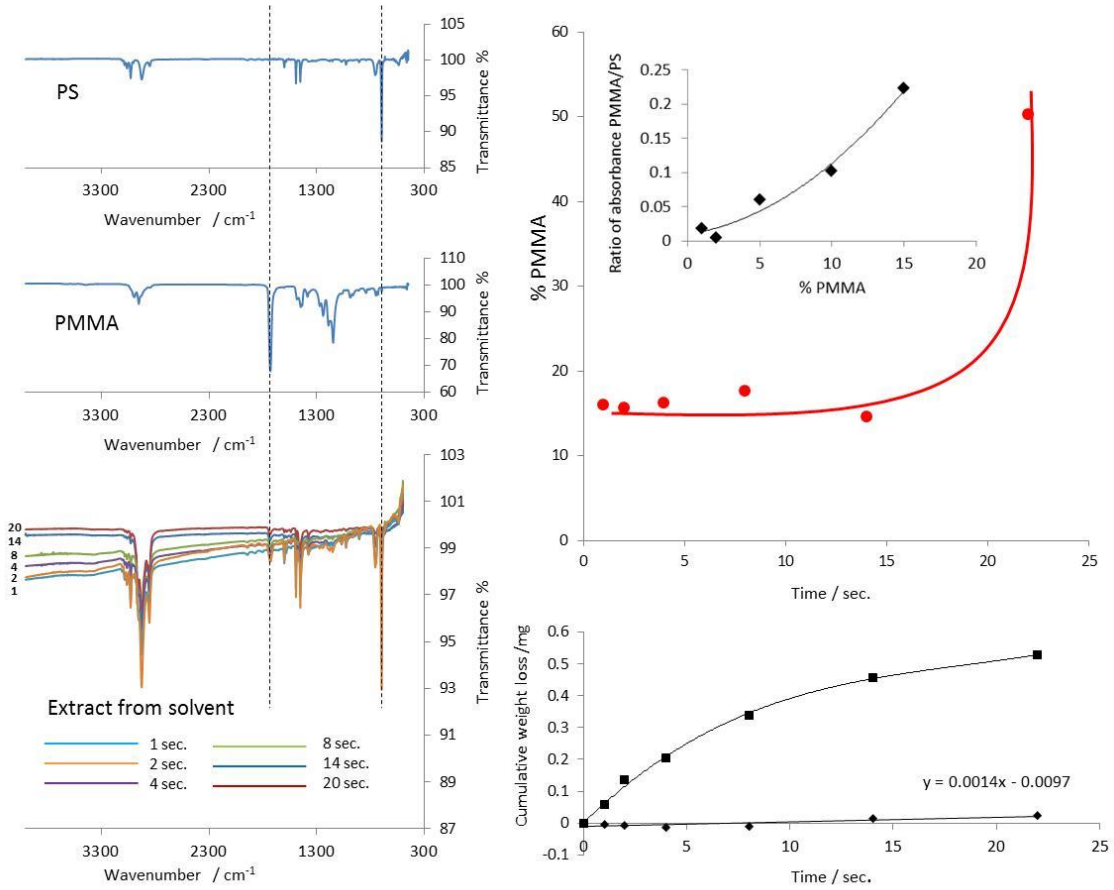

Figure 2. Left; from top to bottom, spectra of pure PS and PMMA then the spectra from the material extracted from the solvent placed on the sample surface. Right, from top to bottom, % of PMMA in the extract (inset is the calibration graph) then the gravimetric data for the blend, squares, and the pure PMMA, diamonds.

EXPERIMENTAL SECTION

Sample Preparation and Imaging. PS and PMMA were both from Aldrich Chemical Co. (PS: Mw = 2.40 x 10E^5 g/mol, PMMA: Mw = 1.03 x 10E^5 g/mol (determined by GPC))**.** The blend was composed of 30% w/w PS and 70% w/w PMMA. The sample was cast from solution in cyclohexane onto a glass substrate, and then conditioned in a vacuum oven at 40^{o}C for one week. The AFM used was a Veeco (now Bruker) Explorer fitted with a high resonance frequency (HRF) silicon probe. The sample was imaged in the tapping mode (TM-AFM). Films of pure PS and PMMA were made in the same way.

Sample Dissolution and Chemical Analysis. For the AFM imaging studies, a single 20 µl drop of cyclopentane was delivered onto the sample surface using a fine pipette and, in the case of the AFM imaging experiments, removed using a one second burst from an air-duster after the required exposure time. The mouth of the tube delivering the pulse of compressed air was held 1 cm away from the droplet at a 45^o angle. In order to ensure that approximately the same area was imaged each time, the sample remained within the base of the AFM thus it was not possible to collect the removed solvent for subsequent analysis. In a separate series of experiments the solvent was applied in the same way and then substantially removed with the same pipette before applying the air-duster. The reclaimed solvent was evaporated to dryness and the dry weight recorded. Samples were then analyzed by FTIR spectroscopy in the transmission mode. Two drops of cyclopentane were used to dissolve the sample which was then transferred onto a NaCl window and allowed to evaporate for ~ 5 minutes. Reference data were collected for films composed of the pure polymers as well as the blend. A calibration graph for the relative concentrations of the two polymers was obtained using the same procedure, except solutions with known concentrations of PS and PMMA were analyzed. The spectra were obtained from 450 to 4000 cm^{-1} at 2 cm^{-1} resolution setting and accumulation scans of 64. The FTIR and gravimetric data are presented **in Figure 2**. The spectra for the two pure materials each have a strong peak that is located in a region where the other has low absorbance; wavenumber 1729.5 cm^{-1} for PMMA, corresponding to its carbonyl group, and 698 cm^{-1} for the PS, corresponding to ring out-of-plane deformation. A calibration graph was created by dividing the absorbance at 1729.5 cm^{-1} by that at 698 cm^{-1} and plotting this ratio.

RESULTS AND DISCUSSION

Sample Dissolution and Chemical Analysis. Figure 1 shows the image of the sample at the start of the experiment and after subsequent exposure to the solvent. At the start, a raspberry-ripple type structure is seen with elongated raised features within a flat matrix. After exposure to the solvent, inspection reveals that raised areas are disappearing leaving pits, or trenches, in their place. This is occurring at different rates in different places. The picture is consistent with the progressive removal of a material that is soluble in

cyclopentane, leaving behind material that is not soluble. The spectra for the material captured from the blend (**Figure 2**) suggest that it is dominated by PS and the quantification confirms that the amount of PMMA remains at about 15%, until after 15 seconds when a relative increase seems to occur due to near-exhaustion of the PS; although the amount removed at this point is small thus the error in this measurement is high, the gravimetric data demonstrate that almost all of the soluble material has been removed by 15 seconds and it is the data before this that are most relevant to the interpretation we offer. The amount of PMMA found in the solvent captured from the blends is greater than the gravimetric curves suggest which implies that some PMMA is entrained with the PS as it leaves the surface. We return to this point below.

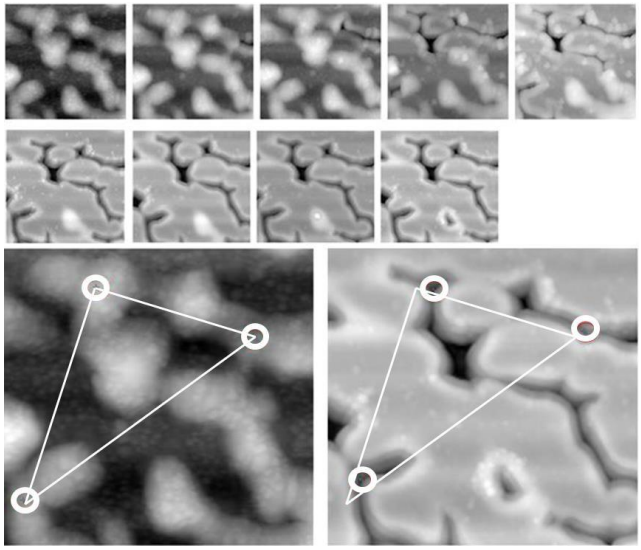

Figure 3. Top (small images) topographic images of the selected area after exposure to the solvent for, from left to right, 0, 1, 2 ,4 ,6 ,8 , 10 , 12 and 15 seconds; note that features drift relative to the frame of the field of view in successive images. Bottom (large images) left, topography of the untreated sample and, right, the topography after 15 seconds exposure to the solvent. The centres of the white circles indicate three points that are chosen as being the same position in the two images. The white triangle joins these points for the first image and this shape is located in the same place relative to the edges in the second image; the drift can be clearly seen. All images are 5μm x 5μm.

This result underlines the importance of analysing the solvent; it is not sufficient to assume that only the soluble material is removed and the insoluble component remains. It is easy to envisage how PMMA could be occluded within the PS and, therefore, be removed by the solvent. Nevertheless, in this case, the overwhelming majority of the removed material is PS.

The gravimetric data for PMMA dissolution does exhibit significant scatter and has to be considered as semi-quantitative, however, the slope of the curve provides an estimate of the rate of loss of the PMMA that is adequate to illustrate our method. The slope implies a rate of loss of 1.4 μg/s (**Figure 2**). The measured diameter of the solvent drop was 12.5 mm with a SD of ±0.96 over 9 measurements. With a density of 1.19 g/cm^3, this leads to an estimate of the rate of removal of PMMA of 2.4 nm/s. The solvent applied to the pure PS film caused a hole to appear with the first application that then increased in diameter. This behaviour was inconsistent with that of the other samples which remained substantially intact up to 15 seconds. Given that the behaviour of the PS was radically different from that of the PMMA and the blend, the results for the captured material are not presented for comparison. Nevertheless, it is clear that the solubility of PS is orders of magnitude greater than that of PMMA.

Imaging during the Process of Surface Dissolution. We know that there are two materials in the sample shown in **Figure 1;** the images suggests two phases (thus little or no mixing at a molecular level), one of which has formed the raised features. From this image, it appears there are roughly equal amounts of both. This is, perhaps, surprising because the sample comprises only 30% w/w PS. Consequently, we start with a significant degree of uncertainty regarding the sample's morphology.

As mentioned above, exposure to the solvent changes the sample's structure and holes, or pits, begin to appear, replacing the raised structures as a consequence of sequential exposures to the solvent. Close inspection of these micrographs reveals that there is significant drift, i.e. the same features appear in different positions at different times. This is to be expected, the sample and stage are subject to forces and temperature changes during the process of exposing the surface to the aliquots of solvent; at high magnification, this inevitably leads to drift between images and even during imaging. The first step in the CIDA process is to remove this drift.

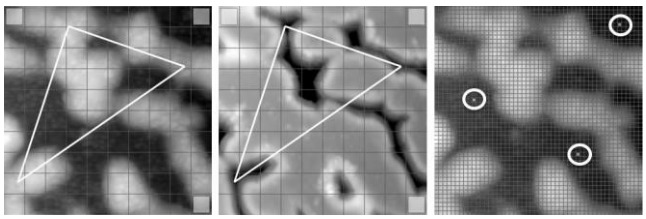

Figure 4. Left, the untreated surface, middle, the same area after 15 seconds exposure. Note that the drift seen in Figure 3 has been substantially eliminated by the software as demonstrated by the white triangles (see **Figure 3** for comparison). These images have been divided into a small number of cells to maintain clarity. Far right, the image is divided into a grid of 50 x 50. The filled-in cells at the centre of the white circles, denote those that were selected as being the same material that will dissolve in the same way. These positions were then used to align the images in the z axis.

Image processing to account for drift in the topographic micrographs. For the sake of clarity we will illustrate correcting for drift using only the first and last images, as shown in **Figure 3**. Our software allows for three points to be selected on each image that are judged to be in the same positions in both images. These are then translated in x and y so that, as **Figure 4** shows, the images are substantially coincident. The next requirement is to align the images in the z-axis. The first step is to divide the images into a grid of cells (in this case 50 x 50), see **Figure 4**. This is important because operating at the level of a single pixel would produce a great deal of noise and too many kinetic plots to process in a reasonable time (see below). When this is done, three cells are chosen that are deemed to be the same material and behave in the same way during exposure to the solvent. Typically the phase chosen would be the least soluble, as in this case, where cells are all sited on the flat areas that change very little, but the method works using any three cells provided the behaviour is the same in all three. The images are then shifted so they are now aligned in the x, y and z-axes. **Figure 5** shows the change in height for each cell where all plots are shifted to be zero at the start. Zero gradient corresponds to no change relative to the cells selected in **Figure 4** and a negative gradient represents a relative decrease in height. A histogram of these gradients is also shown in **Figure 5**.

2D imaging from local kinetic measurements. We continue with the simplified approach that uses only the first and last images, i.e. the large micrographs shown in **Figure 3**. When inspecting the histogram in **Figure 5,** we expect there to be no positive gradients if we have selected cells with the lowest solubility from **Figure 4**; the existence of positive gradients can be regarded as a measure of the noise in the data. In **Figure 5**, it is shown how symmetry allows us to estimate the distribution for the error in the 'unchanged' cells

(more accurately, these are cells that have either not changed or have changed in the same way as the reference cells but, for convenience, we will refer to them as 'unchanged' cells).

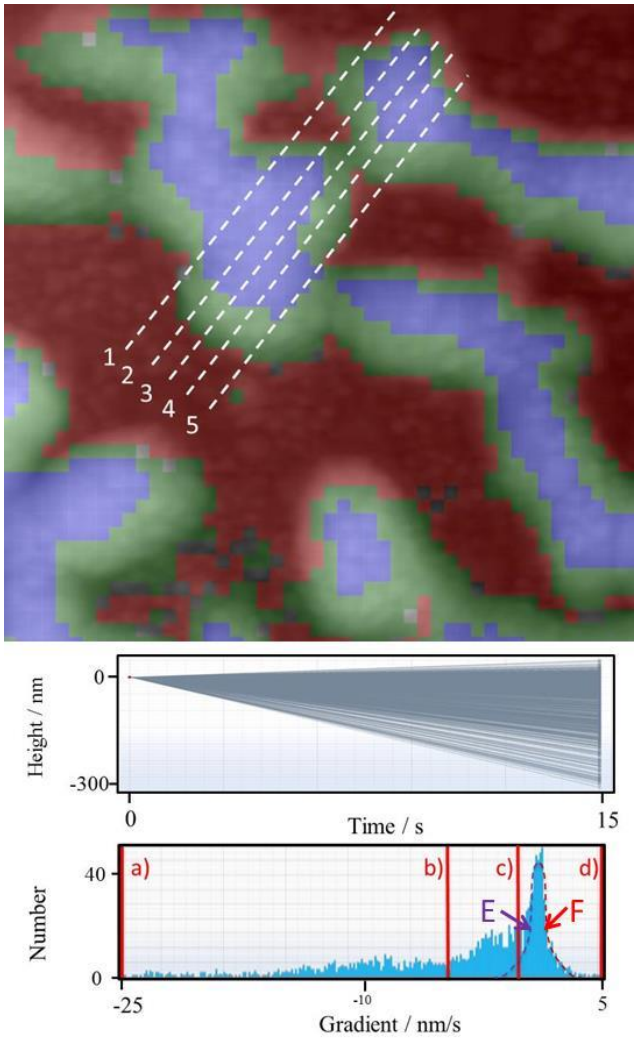

Figure 5. The height vs time graph gives the plots of height change from untreated to 15 seconds exposure in each cell. The starting position for each cell has been set to zero. Underneath is a histogram of these height changes; a trimodal distribution can be seen. The red dashed line, F, encompasses all of the positive values; in this case these give a measure of the error in the measurement as no cells increase in height. The mauve dashed line, E, is a reflection of the red dashed line; together they estimate the error in determining those cells that do not, to a first approximation, change. All cells between a) and b) are coloured blue in the image shown (colour overlaid on topography image, the scale is 5µm x 5µm), cells between b) and c) are coloured green and those between c) and d) are red. This corresponds to blue = greatest change, green = some change and red = no change. Blue and green together map the cells where the raised features have dissolved, i.e. they must be almost entirely composed of PS. The green cells are where the height reduced to the level of the red cells. The blue cells are those where the dissolved phase created a hole or pit. The red cells are PMMA. The white dashed lines on the image are explained in Figure 7.

The behaviour appears to be trimodal with one population being unchanged. We can divide the cells into three categories as shown in **Figure 5**. We can see that the blue + green area, representing the dissolved PS phase, is mapped accurately. The cells where there has been a loss of material, down to the level of the unchanged cells, are coloured green. Where the loss of material caused a trench or pit to be formed is shown in dark blue. Although this is a simple example, it illustrates the principle that we can map where dissolution has occurred, analyse the resultant solution, and then assign an identity to each cell. To a first approximation, in this case, all dissolved material is PS (we will refine this observation later).

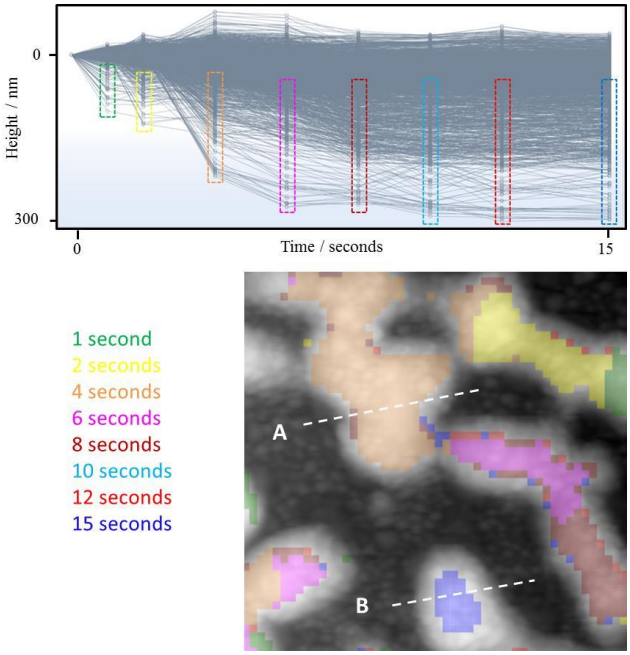

Figure 6. The top graph is equivalent to the similar plot shown in Figure 5 except all 8 images have been used. Cells that have changed significantly in height after 15 seconds exposure to the solvent are captured by the blue box made of dashed lines (this box is drawn by the user using the curser), all of these cells are coloured blue. The red dashed box captures all cells that have changed after 12 seconds, these are coloured red (overwriting the blue); the cells that have changed after 15 seconds but not after 12 seconds remain blue. This process is repeated and, in this way, the cells that have changed significantly from 12 seconds to 15 seconds are identified, then those that have changed from 10 seconds to 12 seconds etc. are identified with corresponding colour coding. The scale of the image is 5µm x 5µm. The white dashed lines are explained in Figure 7 and 9.

We have moved beyond what simple inspection affords, the assignment for each cell is based on a quantitative measurement of dissolution behaviour and we can quantify the volume of material dissolved within the field of view. We can also assign colours to the three different types of behaviour seen in the histogram (**Figure 5**). To a good approximation, the red cells do not dissolve (or more accurately do not dissolve more than the selected cells) and these can ascribed to PMMA, the green cells are those that dissolve to reveal the flat surface of the PMMA and the dark blue cells are those where the PS dips beneath the surface. Inspection of **Figure 4** confirms that the mapping is substantially accurate. Our procedure enables subtle differences in dissolution behaviour to be mapped with high spatial resolution. To our knowledge, this is the first nanoscale image where contrast is achieved through differences in quantified localised kinetics. In this case we have focussed on dissolution kinetics but this capability could be extended to any kind of surface reaction that leads to relative decreases or increases in height.

We can now extend the alignment and analysis to include all of the images shown in **Figures 1 and 3**. The kinetic plots from all the cells for all of the images are given in **Figure 6**. At this point, we are considering 20,000 kinetic measurements. This underlines why

we need to divide the images into cells, as illustrated in **Figure 4**, otherwise the number of measurements would potentially be higher by an order of magnitude or more and the noise from minor errors in the alignment process would be large. Inspection of **Figure 1** indicates that there is little change, then the sudden appearance of a trough or pit; we can map the time at which this sudden change occurs. The procedure for colour coding is given in the caption for **Figure 6,** together with the resultant image. The coloured map is in good agreement with the behaviour implied by **Figures 1 and 3**. This poses the question, "given that the dissolved material is almost entirely PS, why should there be this large range of behaviours such that the step-change can occur at 1 second to 15 seconds?" This is discussed below in the context of the tomographic images.

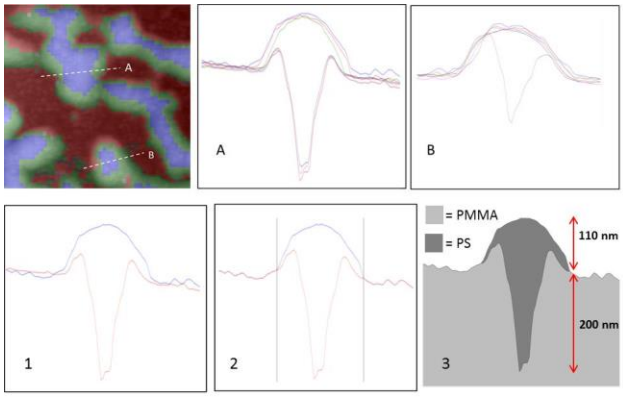

Figure 7. Top left, compositional map taken from Figure 5; red = PMMA and blue and green = PS. Top middle and right; linescans taken from positions A and B in the compositional map for successive exposures to solvent (the same as is shown in Figure 6). For A, the step-change in height occurs at 2 sec., for B the change happens after 15 sec. The tomographic slice is created by a three step process shown in the bottom row; 1 - the linescans for the untreated surface and the same position after the step-change occurred are co-plotted, 2 - two positions delineating the edges of the raised feature are selected (the vertical lines in 2) and within these limits the two lines are preserved and outside only the untreated line is used, 3 – the phases are greyscale-coded.

Construction of Approximate Tomographic Images. To a first approximation, because the polystyrene (PS) is far more soluble in the solvent that the poly(methyl methacrylate), (PMMA), comparison of the starting topography with that after the PS has been substantially removed, provides the basis for understanding the structure as a function of depth. In **Figure 7**, two positions marked on the 2D compositional map are shown as a series of linescans for the successive exposures to solvent. The capability to show the same position in each image follows from the x, y and z axes alignment process. In the case of 'A', a step-change increase in depth is seen after 2 seconds exposure. In the case of 'B', it occurs after 12 seconds exposure; the reasons for the differences are discussed below. The three step process for constructing an approximate tomographic slice is illustrated in **Figure 7**. The linescan for the untreated sample is co-plotted with that for the maximum duration of exposure. The experimenter then decides on the boundaries between the two phases; this choice is guided by the topographic image of the untreated sample. Within the selected limits, the line from the final image is used together with that from the first image, but only the line from the first image is used outside these limits. This then leads to the creation of the first approximation of a tomographic slice.

In **Figure 8** more tomographic slices are shown taken from **Figure 5**. It can be seen that multiple features can be imaged. When a sequence of such maps is obtained by shifting the linescans by equidistant steps, body-scanner type tomography can be performed. In this way we can acquire a detailed understanding of the 3D structure of the sample. .

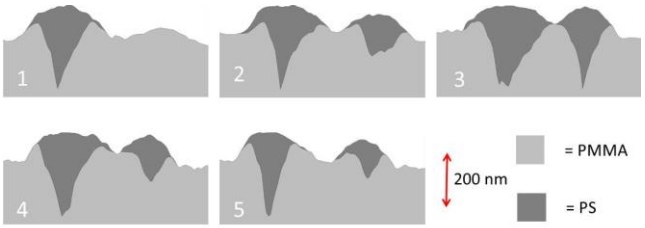

Figure 8. These tomographic slices come from the positions indicated in Figure 5. These are in a sequence that is spaced uniformly thus they are the same as the familiar body-scanner type tomography.

This construction is based on the simplifying assumption that the PMMA does not dissolve/erode significantly and that there is no inaccessible, occluded PS buried beneath the surface and is thereby afforded protection from the solvent by a thick layer of PMMA. Whether these assumptions are tenable can be tested: the rate of dissolution of the less soluble phase can be measured (and this has been done in this case, see above). The total amount of PS in the blend is known (or, more generally, can be measured); inspection of the 2D and 3D images suggests that the simple construction accounts for the PS known to be in the sample, thus there is little occluded polystyrene.

Construction of tomographic images using kinetic data. Above, a methodology was described for 2D mapping of surface composition (with the option of some depth information) on the basis of measurements of the kinetics of dissolution. This same approach can be applied to mapping composition as a function of depth; this is shown in **Figure 9**. Histograms of the height change between successive exposures can be obtained. When these differences are small, the entire dissolved layer can be attributed to the least soluble component then greyscale coded accordingly. When there are combinations of small changes and larger changes, the histograms can be used to determine which positions correspond to the less soluble phase and which to the more soluble phase. Some judgement is required because of the noise in the data but, broadly speaking, the gradient (rate of dissolution) of the least soluble phase is known, so faster rates belong to a different category (and by extension of this approach, multiple phases with multiple rates of dissolution can be categorized with a possible additional variable being the type of solvent used for each exposure). This is illustrated by A and B in **Figure 9**. It can be seen that the PMMA layers on either side of the PS domain now have a depth because the decrease in height has been calculated to be 2.4 nm/s , see above. This can be contrasted with the representation in **Figures 7 and 8** where it has been assumed that the PMMA is completely insoluble. **Figure 9** gives a more realistic picture of the reach of the experiment; it has not probed far beneath the surface of the PMMA but it has done so to some extent. Furthermore, **Figure 9A** shows that the decrease in dissolution rate, after the rapid dissolution event, identifies a layer of PMMA surrounding the base of the PS structure. This is not seen in **Figure 9B**, thus it is probable that all of the PS was not dissolved in this case. These tomographic slices illustrate, in a striking way, the differences between the two positions; there is little removal of PS for up to 15 seconds at B even though PS is highly soluble in cyclopentane. At position A, rapid dissolution starts after 2 seconds. The tomographic images clearly suggest an explanation; there is a layer of PMMA over the surface of the entire sample and this layer has different thicknesses in different places. Inspection of the image in **Figure 6** adds credence to this theory because it is

clear that adjacent regions on the same raised feature follow sequentially. The feature located in the top right of the image changes from green (step-change after 1 second) to yellow (step-change after 2 seconds) then to orange (step-change after 4 seconds). The feature located bottom right goes from dark red (step-change after 8 second) to mauve (step-change after 6 seconds). We do not see a green area (step-change after 1 second) located next to a dark blue area (step-change after 15 seconds). This is exactly the type of behavior that would be expected when there is a PMMA layer over the PS because it is very unlikely there would be acute changes in thickness. This theory also goes some way toward explaining the higher-than-expected amount of PMMA entrained by the solvent. It is easy to envisage that a layer on top of a PS feature would be penetrated in one place before the rest, perhaps near the periphery of the PS domain. The subsequent egress of PS could remove associated PMMA.

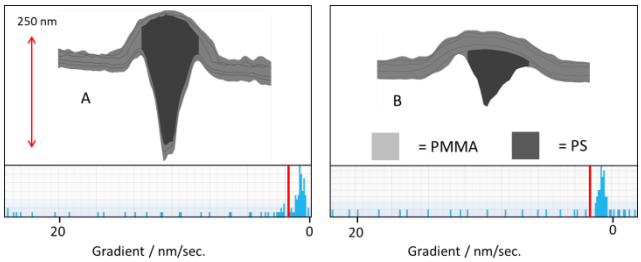

Figure 9. These tomographic slices correspond to the lines A and B that feature in Figures 6 and 7. The greyscale coding shows the time at which the step-change decrease in height occurs. The histograms represent the decrements between 2 and 4 seconds for A and between and after 15 seconds for B. The red lines represent the boundaries; below the greyscale coding is dark grey (PS), above it is light grey (PMMA). Elsewhere the histograms always indicate only a slow rate of dissolution .For A, the kinetics suggest a thin layer of PMMA over the PS while for B the layer is much thicker.

Overview of 2D and 3D imaging. We have described how 2D Chemical Mapping can be obtained from AFM images taken after a series of exposures to a solvent. With suitable software (that allows correction for drift), an image can be divided into a grid of cells and the height change or relative height change within each cell can be measured as a function of exposure. In this way the amount of material lost from the surface can be mapped and plotted as a function of time of exposure and local kinetics can be mapped on a nanoscale. By analysing the material dissolved in the solvent and correlating this with the material lost from the surface, 2D nanoscale compositional maps were created. These same principles can be applied as a function of depth. The nature of the material in each cell can be deduced from the rate at which its height decreases. In a simple analysis, the least soluble phase is assumed not to dissolve and the user identifies boundaries between phases on the basis of an inspection of the topographic images. Comparison of linescans before exposure to solvent and after sufficient exposure to substantially remove, in this case, all of the PS, leads to an approximate tomographic slice. This method can be very useful for gaining an understanding of the 3D structure of a sample in simple cases.

A more sophisticated analysis uses the kinetics of the loss of material as a function of depth. At each exposure, the rate of loss of height is used to categorise the material. This then leads to a tomographic image that does not rely on an assumption that there is a phase that does not dissolve (only that the reference cells behave in a consistent manner) and does not require the user to identify physical boundaries. This approach can map occluded material.

In this study, a single solvent was used and the composition of the sample was known in advance. However, unknown materials are routinely analysed in great detail using conventional analytical methods. Once the composition is known, solvents can be selected for the chemical imaging by dissolution analysis (CIDA) process. Here we have used only one solvent but, our experiment could be extended by using a second solvent that preferentially dissolves the PMMA; in this way any shielded PS would be exposed. It follows that our approach can be generalised to deal with more complex structures where solvents can be found that enable components to be dissolved at significantly different rates (it is not necessary that there is one component that does not dissolve at all). It is reasonable to expect this requirement will be achievable in most cases as changes in molecular structure will typically imply a change in dissolution behaviour. This is also true of changes in physical structure such as the differences between crystalline and amorphous forms of the same material. In principle, therefore, the CIDA approach could be applied to materials with complex structures. Furthermore, it is not limited to organic materials. Metals could be analysed using different reactive solutions that preferentially etch one material more than another; a similar comment applies to ceramics. Biological systems pose greater challenges but highly specific bonding and bond-breaking reactions can be used and both the additional and removal of molecules could be analysed using the principles of CIDA. We will present examples of these capabilities in future articles.

An advantage of CIDA is that it requires no sample preparation. Almost any surface can be exposed to a solvent or a reactive fluid in a controlled way. There is a need that material be removed gradually. If multiple components are removed in a single exposure then interpreting the results could be problematic. Careful selection of solvents and adjusting times of exposure, temperature and rate of flow will, in most cases, enable the removal of material from the surface to be carried out progressively so that every component is removed in a step-wise manner. When multiple components are dissolved in a single step, the analysis of the solvent would detect that this has occurred and, therefore, that the dissolution regime may require refinement.

An important aspect of our method is that any analytical technique can be used. Often combinations of techniques could be employed to analyse the contents of a single solvent aliquot, for example both IR and Raman spectroscopies. A particularly powerful analytical approach is high performance liquid chromatography coupled to mass spectroscopy (HPLC-MS, including tandem MS etc.). This provides a step-change improvement in analytical specificity compared to the vibrational spectroscopies now available for nanoscale imaging such as photothermal IR spectroscopy (often called AFM-IR or Nano-IR) and scattering NSOM Raman and IR spectroscopies. Examples of the use of chromatography with nanoscale mapping will be given in future publications. By adding the ability to analyse composition with chromatography (thus the ability to separate mixtures) as a function of depth, we will have achieved all four of the desirable capabilities listed above.

Notwithstanding issues of analytical power, it might be argued that scattering NSOM spectroscopies[1] could be used to obtain similar results to those obtained in this work because, in this case, we have relied solely on IR spectra. However, the depth of penetration of circa 20nm, would lead to a confusing picture when scanning the surface. The thickness of the PMMA layer covering the PS phase varies from a few nm, corresponding to an step-change in dissolution rate after 1, 2 and 4 seconds, to 29nm for 15 seconds exposure. It follows that the raised features, where we know most of the PS is located, would vary from appearing to be pure PMMA to being dominated by PS, in line with the colour cod-

ing given in **Figure 6**. Thus, the important fact that the raised features are mostly composed of PS that extend to a depth of about 200nm would be lost. If the film were sectioned, then tomographic images such as those shown in the figures in this article might be obtained but sectioning is often difficult, it might destroy the structure that is the object of study and the 'body scanner' type of imaging shown in **Figures 5 and 8** would not be achievable because obtaining a series of sections where exactly the same region is imaged would not be possible in practice. The situation for thermomechanical photothermal imaging[6] (also known as AFM-IR or Nano-IR) is potentially worse. The commercially available form of AFM-IR/Nano-IR is based on that of Hill et al.[6] The first paper on this technique[6] demonstrated that the signal detected at the surface contained substantial contributions from material as far as 500nm below the surface, possibly significantly more. This depth information cannot be properly interpreted, i.e. the depth of the material contributing to the measured signal is not known, therefore, subsurface structure cannot be determined. The spectra would show that the raised features contained both PS and PMMA but the morphology of the sample would remain uncertain. The structure of sections through the sample would remain inaccessible for the same reasons. One consequence of this is that the lateral resolution for this technique cannot be better than the depth probed except in rare cases where all interfaces are normal to the surface.

A key underlying weakness of all of the established approaches is that they are predicated on the need to achieve an individual chemical analysis for every voxel; in the example given in **Figures 6 to 9**, this would equate to 20,000 spectra. Imaging is possible based on this large number of spectra when using conventional FTIR microscopy with focal plane arrays that capture multiple spectra in parallel but there is currently no prospect of a similar approach being possible with SPM-based imaging. Spectra typically take minutes, even with a 1 minute acquisition time, completing a tomograph with the same number of voxels available in the images discussed here would take approximately 14 days. The CIDA data were acquired in a few hours. It is true that there is, in terms of number of data points, far more information in a theoretical 20,000 voxel IR tomograph, however, there is the question of how many different materials might be possible to usefully map in a single experiment? 100 would be a large number which means there is a redundancy of over 2 orders of magnitude in the spectrum-per-voxel approach. CIDA challenges this paradigm. For most real-world samples, the field of view in a typical experiment will contain only a few materials. If, over a large area, this ceases to be true, then the area exposed to the solvent/reagent can have sub-micron dimensions by using nanopipettes. CIDA is a method of assigning every voxel to a particular category, i.e., where there are 'n' materials there will be 'n' categories. The number of materials can be determined by, for example, HPLC-MS; categorization can be achieved using dissolution kinetics (or, in the case of etching for example, reaction kinetics). In this way, tomographs with tens of thousands of voxels can be acquired in a relatively small amount of time. This is the new paradigm we are introducing with CIDA. It brings with it the advantage that the analytical power that can be brought to bear to identify each material is much greater than vibrational spectroscopy alone can provide.

No analytical method is universally applicable and CIDA is no different. Some materials, like cross-linked polymers, might be impossible to dissolve. There will be cases where components have, to within experimental accuracy, the same dissolution kinetics regardless of the solvent used. However, CIDA represents a new approach to nanoscale 3D chemical imaging that might have significant advantages compared to other methods. This may be of particular significance in some cases, particularly in respect of analytical specificity and accurately characterising sub-surface structure.

CONCLUSIONS

Chemical Imaging by Dissolution Analysis or CIDA provides a new paradigm for 2D and 3D imaging down to a nanoscale. It can provide all of the desirable capabilities suggested at the start of the article, no other SPM-based analytical technique can do this. It can be applied to any sample where it is possible to remove material from the surface in a gradual step-wise manner. Typically this would be achieved by using solvents or chemical reactions such as those used for etching metals. The 3D chemical maps allow tomography in a manner similar to the well-known 'body scanner' type imaging but on a nanoscale. We envisage that there will be a very broad range of applications for this new approach.

ACKNOWLEDGMENTS

Muhammad U. Ghori would like to thank University of Huddersfield for funding for a post-doctoral fellowship under the University's Research Fund.

REFERENCES

(1) Smith, B.C. *Fundamentals of Fourier Transform Infrared Spectroscopy*, 2nd ed.; Taylor Francis Group, Boca Raton, FL, USA, 2011.
(2) Dieing, T.; Hollricher, O.; Taporski, J. *Confocal Raman Microscopy*, Springer Series in Optical Sciences, 158, 2011.
(3) Wilson, R. G.; Stevie, F. A.; Magee, C. W. *Secondary Ion Mass Spectrometry: A Practical Handbook For Depth Profiling And Bulk Impurity Analysis*, Wiley, Uni. Michigan, 1989.
(4) Martin, F.L.; Pollock, H.M. *In Oxford Handbook of Nanoscience and Technology*, Vol 2 Ed: Narlikar, A. V.; Fu, Y. Y. Oxford University Press, Oxford, UK, 2010; pp 285-336.
(5) Hammiche, A.; Bozec B.; Pollock, H.M.; Reading, M. *J. Microsc.*, **2004**, *213*, 129-134.
(6) Hill, G. A.; Rice, J. H.; Meech, S. R.; Craig, D. Q. M.; Kuo, P.; Vodopyanov, K.; Reading, M. *Opt. Lett*., **2009**, *34*, 431-433.
(7) Dai, X.; Moffat, J. G.; Wood, J.; Reading, M. *Adv. Drug Del. Rev*., **2012**, *64*,449-460.
(8) Materazzi, S.; Vecchio, S. *Appl. Spectrosc. Rev*., **2011**, *46*, 261-340.
(9) Reading, M. *US Patent US5248199 A*, Filing date 26 May **1992**, Publication date 28 September 1993.
(10) Reading, M. *US Patent US6405137 B1*, Filing date December 30 **1997**, Publication date June 11 2002.
(11) Claybourn, M.; Hammiche, A.; Pollock, H. M.; Reading, M. *US Patent US6260997* B1, Filing date 23 October **1998**, Publication date 17 July 2001.
(12) Reading, M.; Price, D. M.; Grandy, D .B.; Smith, R. M.; Bozec, L.; Conroy, M.; Hammiche, A.;; Pollock, H. M. *Macromol. Symp*. **2001**, *167*, 45-62.
(13) Price, D. M.; Grandy, D. B.; Reading, M. *Proc. 29th North American Thermal Analysis Society*, Sept. 24-26, **2001**, 574-579.
(14) Price, D. *Handbook of Thermal Analysis and Calorimetry, Vol. 5*: Recent Advances and Applications, Ed. Brown, M.E. and Gallagher, Elsevier B.V. 2008.
(15) Tai, T.; Karacsony, O.; Bocharova, V.; Van Berkel, G. J.; Kertesz, V., *Anal. Chem*., **2016,** *88*, 2864-2870.
(16) Harding, L.; Wood, J.; Reading, M. *Anal. Chem*., **2007**, *79*, 129-139.
(17) Reading, M.; Grandy, D.; Hammiche, A.; Bozec, L.; Pollock, H. M. *Vib. Spectrosc*., **2002**, *29*, 257-260.
(18) Dai, X.; Moffat, J. M.; Mayes, A. G.; Reading, M.; Belton P .S.; Grandy D. B. *Anal. Chem*., **2009,** *81*, 6612-6619.

For TOC only